Preparation and Characterization of Monodisperse Fe Nanoparticles

Dorothy Farrell,[†] Sara A. Majetich,*[,†] and Jess P. Wilcoxon[‡]

Physics Department, Carnegie Mellon University, Pittsburgh, Pennsylvania 15213-3890, and Nanostructures and Advanced Materials Chemistry, Department 1122, Sandia National Laboratories, Albuquerque, New Mexico 87185-1421

Received: May 2, 2003; In Final Form: July 16, 2003

Fe nanoparticles prepared by iron carbonyl decomposition using different methods are compared structurally, chemically, and magnetically. The specific magnetization of the particles was determined from the magnetic moment, the particle size observed by transmission electron microscopy, and the total iron concentration found from calibrated X-ray fluorescence. The volume fraction of oxide is reported for particles of different sizes and for particles made by slightly different techniques.

I. Introduction

Monodisperse Fe nanoparticles were prepared under an argon atmosphere, via thermal decomposition of iron pentacarbonyl, $Fe(CO)_5$. Two methods were used, one using platinum seeds to heterogeneously nucleate the iron particles and the other relying on a supersaturation of iron pentacarbonyl to homogeneously nucleate particles. Various synthesis and processing routes were explored to vary the particle size and the type of surfactant coating.

Iron-based nanoparticles have been of interest for fundamental studies of monodomain magnets and have been studied or used for a wide range of applications including magnetic recording, media,[1] ferrofluids,[2] magnetic cell separation,[3] MRI contrast agents,[4] and environmental remediation.[5] Historically there have been three main challenges: controlling the particle size, achieving monodispersity, and minimizing the amount of oxidation. They have been scrupulously controlled at the same time only under high vacuum conditions using a cluster beam source,[6] an approach suitable for fundamental studies requiring only minute amounts of material. With the advances in controlling the particle size through chemical methods that make macroscopic quantities of material,[7] we revisit the Fe system and examine the degree to which it is possible to limit and quantify the oxidation.

Iron particles have previously been prepared by a variety of different methods. Mechanical milling has been used to prepare ferrofluids containing iron nanoparticles in kerosene or similar organic liquids.[2] These particles were dispersed by the addition of a surfactant such as oleic acid to coat the particle surfaces. This approach yields a significant distribution of sizes and shapes, as do gas-phase methods,[8] but provided the particles were not exposed to air, the magnetizations were quite large. For gas-phase-grown Fe particles with an average diameter of 20 nm, specific magnetizations, σ_s, as high as 190 emu/g were achieved,[8] compared with a bulk value of 218 emu/g. To our knowledge, these high-moment monodomain particles have not been dispersed in liquids. Solution chemistry approaches have also been used. There are many aqueous solution methods to prepare relatively monodisperse iron oxide (Fe_3O_4 or γ-Fe_2O_3) nanoparticles, though the particle surfaces may still be irregular (see, for example, ref 9). Though the magnetizations of these phases are lower[10] (74 emu/g for γ-Fe_2O_3 and 84 emu/g for Fe_3O_4), by fully oxidizing the particles, their magnetic properties are stable over time—an important requirement for applications of magnetic particles. Iron salt precursors have also been used in nonaqueous solvents, most notably in the polyol reaction.[11,12] This method can be used to make larger particles, but they contain multiple grains.

A large number of groups have used metal carbonyl precursors. Fe nanoparticles were first prepared from $Fe(CO)_5$ in organic solvents,[13] following a similar approach used to make Co particles.[14] Iron particles with a metal core of 6 nm diameter were found to have an initial σ_s of 82 emu/g, and 16 nm particles had $\sigma_s = 130$ emu/g.[13] Amorphous Fe nanoparticles can also be made provided the temperature is kept low and the decomposition of the carbonyl is stimulated sonochemically.[15] Thirty nanometer particles made this way contained less than 12 atom % carbon and had a magnetization of 173 emu/g.[15] For elevated temperature preparations, the carbon content can be as high as 30 atom %, lower temperatures favoring an increased proportion of carbon.[16] With a large carbon fraction, the annealed particles crystallize at temperatures as low as 250 °C to yield mixtures of α-Fe and various iron carbide phases.[17] The presence of ammonia during the synthesis can lead to the less-oxidation-sensitive ϵ-Fe_3N phase, if it is abundant.[18] The specific magnetization of particles made with $Fe(CO)_5$ and NH_3 was reported to be as high as 140 emu/g of Fe for 30 nm particles, based on iron masses estimated from the precursor feed ratios.[19] It is possible to narrow the size distribution of $Fe(CO)_5$-based nanoparticles sufficiently that, when coated with a surfactant, they spontaneously assemble into arrays when the solvent is evaporated.[7,20]

It is difficult to quantitatively compare the magnetic results for these particles, though all groups have found that larger particles have higher magnetic moments. This could result from a reduced amount of surface oxide, structural differences near the surface and perhaps a higher carbon content, or a reduced fraction of canted spins. This surface, which was once referred to as the "magnetic dead layer", is undoubtedly complex, but recent advances make it possible to understand it in greater detail. Aside from inherent differences in the particles, two

* Corresponding author. E-mail: sm70@andrew.cmu.edu.
[†] Carnegie Mellon University.
[‡] Sandia National Laboratories.

10.1021/jp0351831 CCC: $25.00
Published on Web 09/11/2003

factors can introduce errors in the magnetic measurements. The first is that these particles oxidize readily with even small partial pressures or brief exposures to air. While there are standard handling techniques that make it possible to transfer a sample for magnetic measurement without exposure, it is harder to determine the degree of oxygen exposure by structural or chemical methods. This makes it difficult to quantify the affects of chemical impurities, structural disorder, and spin canting. The value of the specific saturation magnetization assumes that the mass of iron in the samples is known, but this is quite difficult to determine. There is a significant amount of surfactant present, but because the particle coverage is not 100%, it is hard to determine the exact amount.

In this paper, we describe the synthesis and structural and chemical characterization of Fe nanoparticles. We report a method for determining the Fe abundance and show that weighing even washed samples yields significant errors. We combine the results of transmission electron microscopy (TEM) and magnetometry to determine the volume fraction of oxide for particles of different sizes. Further experimental results differentiate oxidation that is innate to the preparation method and that which arises even during a brief exposure to air while transferring a sample into the electron microscope.

II. Experimental Methods

A. Particle Synthesis. Monodisperse Fe nanoparticles were prepared under an argon atmosphere via thermal decomposition of iron pentacarbonyl, $Fe(CO)_5$. Two methods were used, one using platinum seeds to heterogeneously nucleate the iron particles and the other relying on a supersaturation of iron pentacarbonyl to homogeneously nucleate particles. Various synthesis and processing routes were explored to vary the particle size and the type of surfactant coating.

A.1. Hetergeneous Nucleation Synthesis. This approach follows a method similar to that of ref 7 but without excess Pt. In a typical heterogeneous nucleation synthesis of 7 nm diameter particles, platinum seed clusters were formed by the polyol reduction of 4 mg of platinum acetyl acetonate, $Pt(acac)_2$ by 150 mg of 1,2-hexadecanediol in a dioctyl ether solution containing 0.5 g of surfactant. The initial surfactant was a 1:1 molar combination of oleic acid (OA) and oleylamine (OY). The solution was heated while stirring to 100 °C, and 0.2 mL of $Fe(CO)_5$ was added. The yellow solution darkened as it was heated past 160 °C, becoming black by 200 °C. The color change indicated the growth of Fe on the Pt seed clusters. Heating continued until reflux at approximately 287 °C, and then the heating mantle was removed, and the solution was cooled to room temperature.

An additional stage of growth followed. After the solution was cooled, the volume of octyl ether was doubled, and the solution was reheated. An additional 1.2 mL of $Fe(CO)_5$ was added at 100 °C, and heating continued until 260 °C, when the sample was again immediately cooled and removed to an argon atmosphere glovebox for washing. The initial heating stage lasted less than 25 min with no refluxing, and the second stage lasted no more than 10 min. The final sample showed ferrofluidic response to a permanent magnet.

To make smaller particles, less iron pentacarbonyl was used. To increase the particle size, larger amounts of iron carbonyl were used and the heating times were longer during both stages. Larger particles were also prepared using reduced amounts of the Pt seeding agent, but this method was less reliable.

To exchange solvents, anhydrous ethanol was added in a 3:1 volume ratio to the octyl ether solution to flocculate the particles. Once flocculated, the particles responded to the gradient of the applied magnetic field and were collected by a permanent magnet. The supernatant was then decanted; the particles were redispersed in hexane. Additional OA/OY was added once at a concentration of 0.05 M to improve the dispersion stability.

The surfactants studied were OA, OY, OA/OY, 1:1 molar mixtures of shorter-chain analogues, hexanoic acid and hexyl - amine, propanoic acid and propylamine, and tributylphosphine and 1,2-hexadecanediol. Only oleic acid (OA) and oleylamine (OY) were used during synthesis because the other surfactants investigated had boiling points lower than the boiling point of octyl ether. When OA and OY are mixed together to make OA/OY, heat is evolved. This is attributed to imide formation when the carboxylic acid group of OA reacts with the amine group of OY, as in the formation of a peptide. We will refer to this linked surfactant as OA/OY. Although both OA and OY are liquid at room temperature, a mixture of the two heated to improve homogeneity solidifies when cooled. To exchange surfactants during the solvent exchange, the concentration of the new surfactant was chosen to match that of the original OA/OY when the particles were redispersed in hexane, typically for 24 h.

A.2. Homogeneous Nucleation Synthesis. An alternative approach follows a technique for making iron oxide nanoparticles[21] but omits the final oxidation stage. In a typical homogeneous nucleation synthesis of 9 nm diameter particles, 2.28 g of oleic acid (OA) was stirred in octyl ether, and the solution was heated. At 100 °C, 0.3 mL of $Fe(CO)_5$ was added in a 1:3 molar ratio to the OA (the OA concentration here is 0.54 M, while that of the OA and OY for the heterogeneous nucleation method are both 30 mM). Following the injection, the solution turned orange by the time it began to reflux (20 min); after another 70 min it turned black. The solution was then cooled to room temperature and moved to a glovebox for solvent exchange.

When a permanent magnet was brought close to the flask, no movement of the particle solution was noticeable. This does not mean that the particles are not magnetic but only that the magnetic forces are much weaker than the viscous forces in solution. Because these fluids did not respond to a magnet, centrifugation was used to collect the particles following ethanol addition. The supernatant was decanted, and the particles were redispersed in hexane without additional surfactant because excess OA sedimented in the sample vial following hexane addition.

B. Structural and Chemical Characterization. *B.1. Transmission Electron Microscopy (TEM).* The primary method for structural characterization was TEM, using a Philips EM420 120 kV electron microscope. During redispersion in hexane, the particle suspensions were diluted from their as-made concentration, generally by a factor of 3−5, although sometimes by as much as 20 times. TEM grids were prepared either by dipping a grid into the particle suspension and holding it aloft to dry or by dropping solution onto the grid with a pipet. Grid preparation was done in a glovebox with 2−7 ppm of O_2 and H_2O.

The samples were imaged using conventional TEM techniques. After the images were digitized, NIH Image 1.6.2 software was used to determine the average particle size and the size distribution. This analysis used at least 500 particles and often over 2000 particles. Particles were identified by the contrast between particle and background, and their edges were outlined. The observed contrast in the images reflects the particle core and not the surfactant halo, which is rarely visible in conventional TEM images. The software measured the particle

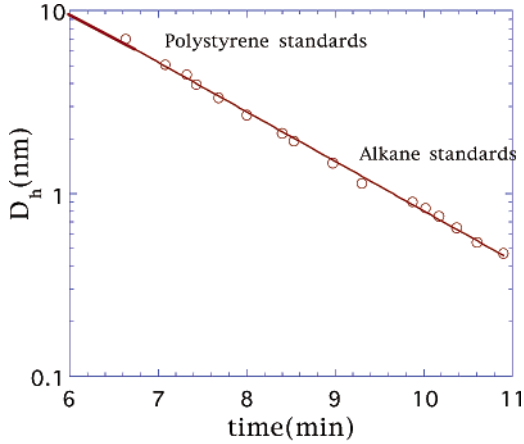

Figure 1. Hydrodynamic diameter vs elution time for polystyrene standards. The best fit (solid line) predicts that D_h (nm) = 413 exp[−0.624t (min)].

along its major and minor axes, and the particle size was taken to be the average. Using Igor Pro software, we fit the data to Gaussian functions to determine the mean particle sizes and standard deviations.

Electron diffraction patterns taken in the TEM were used for phase identification of the materials. Because the grids were exposed to air for brief times during transfer between the glovebox and the electron microscope, additional experiments were done to assess the effect of this air exposure. In some cases, the particles were examined in a flocculated state, and in other cases, the particles were sealed in ampules and annealed at 400 °C for 30 min before analysis.

B.2. Size Exclusion Chromatrography (SEC). SEC was used to examine the average hydrodynamic diameter (D_h) in solution and the size dispersion, and also whether the different surfactants bind irreversibly to the particle surface. A cross-linked polystyrene gel column packed with 5 mm particles containing 1000 Å pores (Polysciences model PL-1000) was calibrated with a series of known molecular weight polystyrene and alkane standards. The calibration plot used to obtain the hydrodynamic diameter of the clusters is shown in Figure 1. The hydrodynamic diameter, D_h, followed the log $D_h \approx t$ scaling shown by the fit (solid line), where t is the retention time in the column. The retention time was measured by absorbance as detected by an on-line photodiode array. We chose the absorbance as measured at 400 nm to detect the elution of the Fe particles. A time of 0.1 min was added to the observed absorbance elution time of the Fe clusters to take account of the time delay between the on-line photodiode array and refractive index detectors, which were used for calibration. Toluene was used as the mobile phase. In some experiments, surfactants were added to reduce the chemical interaction of the Fe clusters with the cross-linked styrene column. These surfactants included oleic acid, hexadecanoic acid, and hexadecylamine.

B.3. X-ray Fluorescence (XRF). X-ray fluorescence using a Spectrace QuantX instrument was used to determine the total amount of Fe from the integrated intensity of fluorescence of the Kα line of Fe at 6.40 keV. X-rays generated by the source are directed onto a fixed volume of the particle dispersion, stimulating re-emission of X-rays by the atoms in the sample. The energies of the emitted X-rays are specific to the elements in the sample, and the relative concentrations of these elements were determined by calibrating the intensities with elemental standards.

The concentrated samples of nanoparticles were diluted with a precise amount of toluene in a glovebox. Enough solution volume (i.e., >3 mL) was used to ensure 100% absorbance of the exciting X-rays in the cells used in this instrument. An ultrathin Mylar window (3.6 mm) allows sensitivity to ∼2−4 ppm for Fe. The concentration vs response curve from 1000 to 10 ppm was nearly linear upon the basis of NBS traceable Fe standards obtained from Alfa Chemicals as metal organic Fe compounds in xylene. These standards gave Kα area peaks that agreed with samples prepared from iron acetoacetonate in toluene to ±5%.

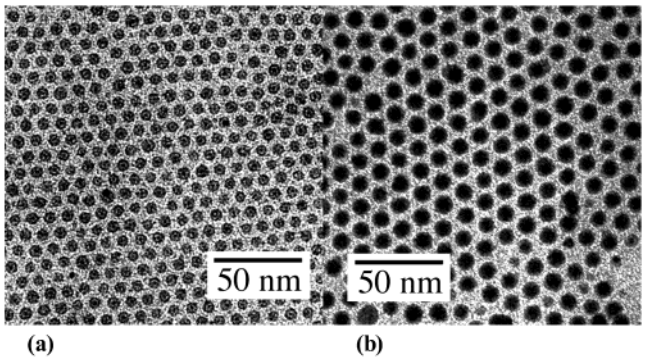

Figure 2. TEM images of heterogeneously nucleated particles: (a) 7.0 ± 0.8 nm (sample Fe101801); (b) 9.2 ±0.7 nm (sample Fe090501).

B.4. Magnetic Measurements. The magnetic behavior of particles in dilute suspensions was investigated using a Quantum Design MPMS superconducting interference device (SQUID) magnetometer. The dilute samples were prepared in a glovebox by dilution of an iron nanoparticle suspension of known concentration. A volume of the sample, generally 0.2 mL, was then transferred by syringe into a glass tube. The tube was sealed under argon using Swagelok fittings attached to a vacuum valve, removed from the glovebox, and flame-sealed with an oxy-acetylene torch to make an ampule.

The magnetic properties of dilute samples of the particles were examined to determine the proportion of iron and iron oxide for 7 and 9 nm particles made by the heterogeneous nucleation method and for 11 nm particles made by homogeneous nucleation. Zero-field-cooled and field-cooled measurements were taken to determine the blocking temperature, T_B. Below T_B, the samples were in their ferromagnetic rather than superparamagnetic state. For zero-field-cooled measurements, the sample is cooled to 10 K in zero field. After stabilizing at 10 K, a 100 Oe field is applied to the sample, and the moment is measured at successively increasing temperatures. The zero-field-cooled curve will show a peak in the moment at the blocking temperature. The field-cooled measurements are made on a sample after it is cooled from room temperature in a 100 Oe field. Hysteresis loops, $M(H)$, were measured between −50 and +50 kOe to determine the saturation magnetization of the particles. These experiments were done at 10 K to ensure that the particles were in their ferromagnetic state.

III. Results and Discussion

A. Particle Size. Typical images of particles made by the heterogeneous and homogeneous nucleation are shown in Figures 2 and 3, respectively. Table 1 lists all samples discussed in this paper and the method used to prepare them. Variations in these synthesis procedures produced nanoparticles with average diameters ranging from 5 to 20 nm. The particle size was most sensitive to the surfactant-to-iron molar ratio and to the maximum temperature. Evidence of Fe nanoparticle formation was not seen in the homogeneous nucleation preparation until the temperature reached the boiling point of the octyl ether.

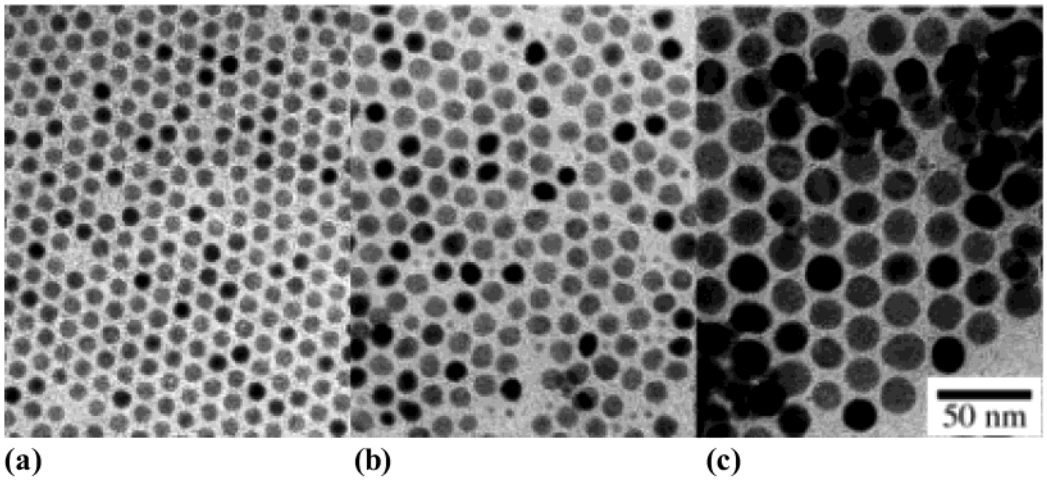

Figure 3. TEM images of homogeneously nucleated nanoparticles: (a) 9.1 ± 0.9 nm (sample Fe040502); (b) 11.2 ± 1.0 nm (sample Fe022602); (c) 19 nm (sample 052002).

TABLE 1: Sample Types and Particle Concentrations

sample name	nucl method	Fe concn (M)	TEM diameter (nm)	particles/ mL
Fe112601[a]	heterogeneous	0.051 (3260 ppm)	5.8 ± 0.5	3.6×10^{15}
Fe070301[b]	heterogeneous	0.0957	7.2 ± 0.5	3.5×10^{15}
Fe010703[c]	heterogeneous	0.0614	8.6 ± 1.6	1.3×10^{15}
Fe021303[c]	heterogeneous	0.080	8.4 ± 1.0	1.9×10^{15}
Fe022602	homogeneous	0.0284	11.2 ± 1.0	
Fe040502	homogeneous		9.1 ± 0.9	
Fe052002	homogeneous		19	
Fe090501	heterogeneous		9.2 ± 0.7	
Fe101801	heterogeneous		7.0 ± 0.8	

[a] Stabilized by hexadecanediol. [b] Stabilized using the OA/OY. [c] Synthesized in Decalin instead of octyl ether.

This has been attributed to the formation of an iron−oleate complex when the $Fe(CO)_5$ is added to the oleic acid solution.[21] The black color associated with Fe^0 does not appear until the solution has aged. In the heterogeneous nucleation method, the Fe^0 forms at lower temperature because there is less oleate to bind to the Fe, requiring less thermal energy to be driven off.

The homogeneous and heterogeneous nucleation methods differed greatly in their ability to synthesize large Fe particles (>9 nm). Using the homogeneous nucleation approach, we could synthesize 11.2 nm particles via decomposition of only 0.3 mL of $Fe(CO)_5$ in the presence of excess OA alone and 9 nm particles in an excess of OY. Particles as large as 19 nm could be made using 0.6 mL of $Fe(CO)_5$ and 2.0 g of OA/OY during each of two growth stages (Figure 3). By seeding the reaction with Pt, we could produce a large number of Fe particles during short reactions, but the size of the particles is limited. Particles 4.8 nm in diameter were synthesized using a total of 1.5 mL of $Fe(CO)_5$ in a two stage reaction with no surfactant present. For the heterogeneous method, the maximum size for monodisperse particles was approximately 9 nm. Here 2.4 mL of $Fe(CO)_5$ was used, the second stage heating time was 2 h, and the temperature was 187 °C. The time at reflux was the determining factor in uniformity of particle shape and the size monodispersity. Heating for 1 h or more during particle growth was needed for maximum size, and an Ostwald ripening period of greater than 1 h was also required. Heating times greater than 70 min, however, had no discernible effect on size but compromised the particle shape for the homogeneously nucleated particles.

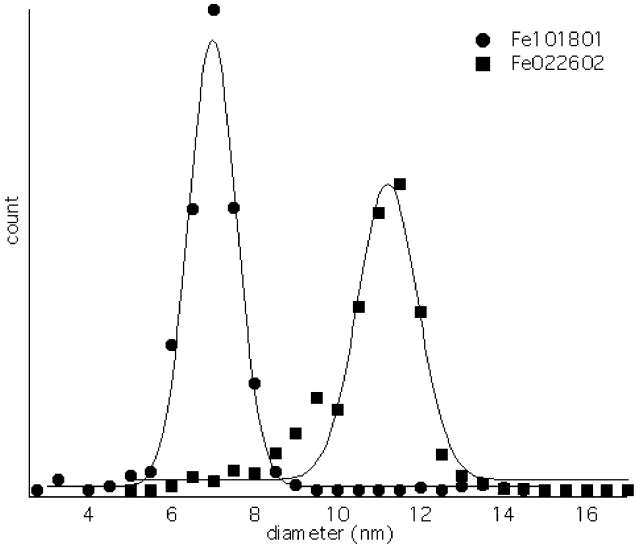

Figure 4. Size distribution plots for particles in Figure 2a (sample Fe101801) and Figure 3b (sample Fe022602).

Figure 4 shows the results for the size distributions of the samples from Figures 2a and 3b. The labels on the distribution plots indicate the date of synthesis of each sample. From the fit, the mean diameter in sample Fe101801 was 7.0 ± 0.8 nm and the mean diameter in sample Fe022602 was 11.2 ± 1.0 nm. Particles with size less than 3 nm, arising from secondary nucleation, were not included in the count for this sample. With sufficient time and temperature, such particles can be dissolved through Ostwald ripening. Here removing these particles caused only slight (less than 10%) changes in average particle size.

B. Electron Diffraction and Particle Phases. Homogeneously nucleated particles coated with OA also displayed greater contrast variation between particles, indicating differing crystallographic orientations (Figure 3). The absence of this variation in heterogeneously nucleated and OY-stabilized homogeneously nucleated particles indicated that these particles have a more disordered structure. The higher temperatures at which the Fe formed in the OA-stabilized particles lead to this improved crystallinity.

Electron diffraction patterns showed enhanced crystallinity in the homogeneously nucleated particles. Figure 5 shows the electron diffraction patterns of the particles of Figures 2a and 3b. The typical pattern of a homogeneously nucleated sample

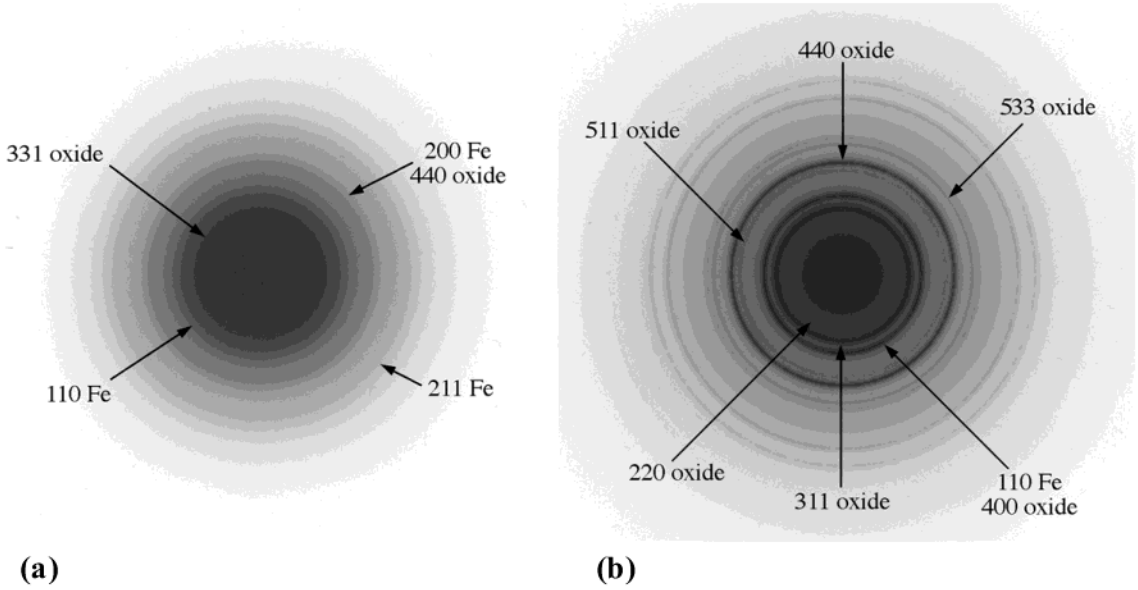

Figure 5. Electron diffraction patterns: (a) heterogeneously nucleated 7.0 nm diameter particles of Figure 2a (sample Fe101801); (b) 11.2 nm homogeneously nucleated, OA-stabilized particles of Figure 3b (sample Fe022602). Rings are indexed to α-Fe and Fe_3O_4.

consisted of three or four diffuse rings corresponding to lattice spacings of 0.255, 0.211, 0.150, and 0.115 nm. The diffuseness indicates that the particles are not highly crystalline. The observed lattice spacings were compared to the (*hkl*) spacings for bcc Fe and fcc Fe_3O_4. The strongest reflections for bcc Fe are 0.203 (110), 0.117 (211), 0.143 (200), and 0.0906 nm (310), and the strongest oxide reflections are 0.253 (311), 0.148 (440), 0.297 (220), and 0.162 nm (511). The observed patterns contain the two strongest oxide reflections and one or two of the strongest Fe reflections. The information from the electron diffraction patterns is insufficient to differentiate the ferrimagnetic oxide phase that is present. γ-Fe_2O_3 and Fe_3O_4 have the same lattice spacings for the first five rings; indexing to the specific phase requires more precise angle and intensity information than is available from an electron diffraction pattern. In many fine particle systems, Mössbauer spectroscopy has been used to differentiate the two possible oxides, and the results are usually consistent with the γ-Fe_2O_3 phase, which has an Fe_3O_4 structure plus an ordered arrangement of vacancies. Unless the oxides have been treated at very high temperatures (>1000 °C) to achieve the equilibrium structure, their vacancy locations are most likely disordered.

Particles that were synthesized by the heterogeneous nucleation method but using extended heating periods had electron diffraction patterns with additional rings at lattice spacings of 0.295 and 0.160 nm, corresponding to strong oxide reflections. Heating also sharpened the contrast in these diffraction patterns, indicating enhanced crystallinity. The patterns for these particles matched well with the patterns from particles of roughly the same size synthesized by homogeneous nucleation in the presence of OY and a longer heating period. The additional oxidation in the heterogeneously nucleated sample suggests that the presence of an oxygen-containing ligand (OA) encourages oxidation of surface Fe atoms.

The electron diffraction patterns of OA-stabilized particles made by extended heating cycles of homogeneously nucleated dispersions differed from those described above. As can be seen in the image on the right in Figure 5, the number of rings increased. The greatest amount of oxidation was seen in particles synthesized with extended heating in the presence of OA, particularly the homogeneously nucleated particles.

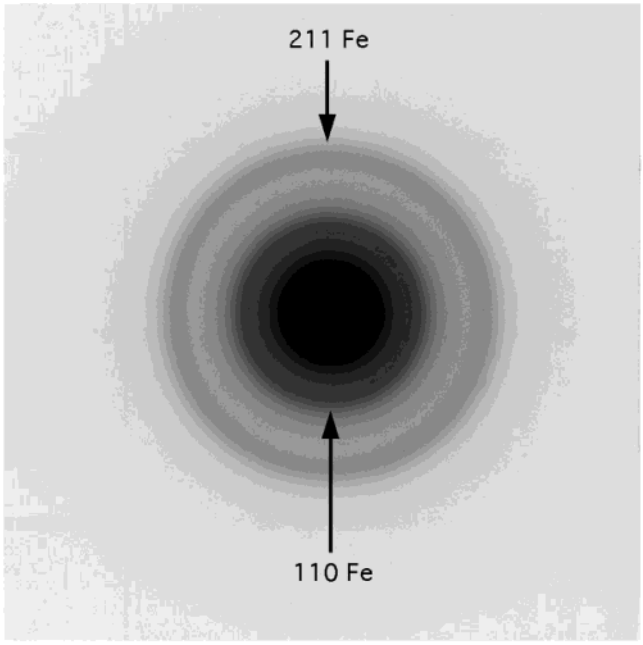

Figure 6. Electron diffraction pattern of propylamine/propanoic acid-coated Fe nanoparticles made by the heterogeneous nucleation method.

The oxidation evident in the electron diffraction patterns could arise either during the synthesis or during a later stage of TEM sample preparation. To determine the origin, the OA/OY surfactant coating of a heterogeneously nucleated sample was exchanged with propionic acid/propylamine, which caused the particles to flocculate. These large agglomerates were partially protected from air by the surfactant shell and less dominated by surface oxidation effects because of their larger volume. Figure 6 shows the electron diffraction pattern of the agglomerates, in which only rings associated with bcc Fe are evident. Standard heterogeneously nucleated particles synthesized without extended heating appear to oxidize after the samples were dried, presumably during transfer through air into the electron microscope.

The least amount of oxidation was seen for heterogeneously nucleated particles coated with tributyl phosphine ligands. These

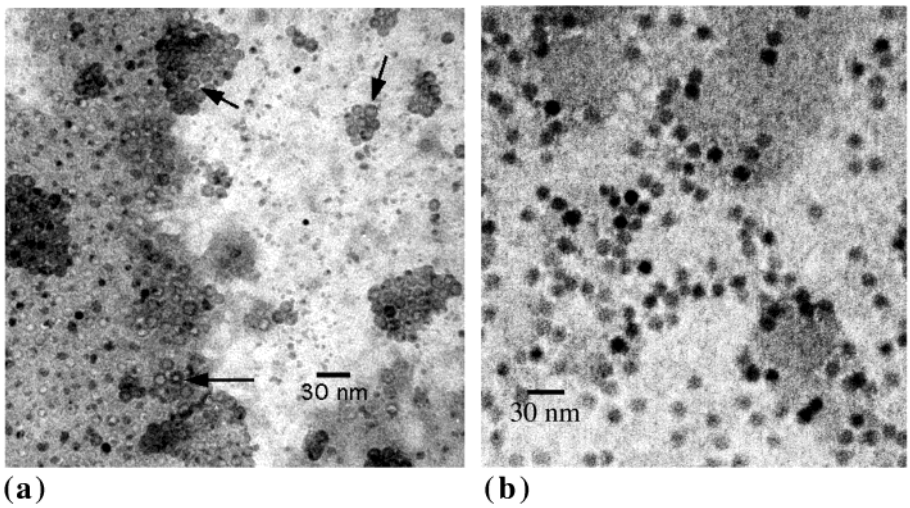

Figure 7. TEM images of annealed tributyl phosphine-coated Fe: (a) annealed 6.7 nm Fe particles made by the heterogeneous nucleation method (arrows point to particles with hollow centers); (b) annealed 9 nm Fe/Fe oxide particles made by the homogeneous nucleation method showing no hollow centers.

particles were studied through a series of annealing experiments performed on heterogeneously nucleated particles synthesized using small amounts of OA/OY and on particles synthesized via homogeneous nucleation using a large amount of OA. The OA/OY coating on heterogeneously nucleated 6.7 nm Fe particles was exchanged with tributyl phosphine to limit available oxygen at the particle surface, and the particles were dried and annealed under a partial argon pressure for $^1/_2$ h at 400 °C. A TEM image of the postannealing particles is shown on the left side of Figure 7. Holes have appeared at the core of the particles, and the particle diameter is larger than that prior to annealing. Particles coated with OA/OY and annealed under the same conditions did not form holes at their centers. Because the annealing temperature is above the decomposition temperature for oleic acid,[22] these particles sintered together, forming large iron oxide crystals.

The morphology of the annealed tributyl phosphine-coated particles suggests that a rapid reaction has occurred during annealing. This is consistent with Fe particles upon exposure to oxygen, which would occur after decomposition and removal of the tributyl phosphine during annealing. The absence of this feature in OA/OY-coated particles suggests that the oxygen from the carboxylic acid groups has begun to oxidize the particle surface prior to decomposition of the surfactant, preventing rapid reaction of the surface with ambient oxygen upon surfactant removal. The results of these annealing experiments also suggest that the amount of OA present during heterogeneous nucleation experiments is not sufficient to significantly oxidize the particle surface unless thermal energy is added to the particles.

Annealing experiments were repeated for a sample of 9 nm particles synthesized via homogeneous nucleation in the presence of excess OA to test for surface oxidation in these particles. The "donut" morphology is not observed for annealed tributyl phosphine-coated particles, shown on the right side of Figure 7, indicating that rapid oxidation of these particles does not take place and that an oxide shell is in place on these particles prior to drying.

C. Size-Exclusion Chromotography and Hydrodynamic Particle Size. The hydrodynamic diameter, D_h, found from size-exclusion chromatography will typically be larger than the inorganic Fe core size as measured by TEM because of the presence of the organic ligand on the surface. However, this depends on whether the OA/OY ligand binds irreversibly to the Fe clusters during the HPLC experiments or whether dynamic exchange between bound and unbound surfactant occurs. As we discuss subsequently, the latter seems to be the case because either a primary amine or the OA/OY must be present in the mobile phase to allow elution of the Fe clusters. This is not the case for thiol-ligated Au clusters.[23]

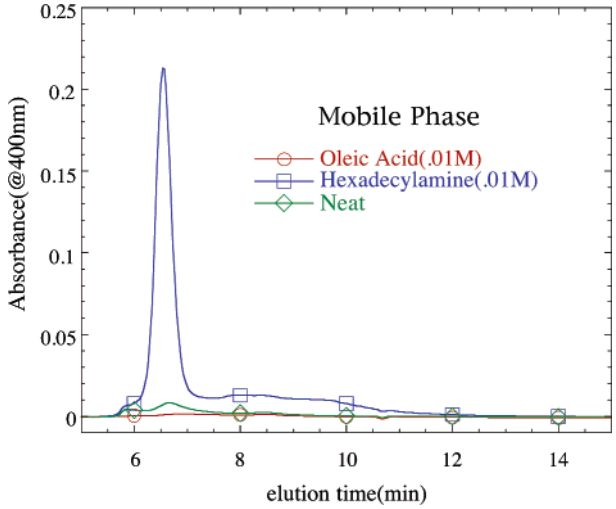

Figure 8. Absorbance chromatogram of sample Fe070301 of which the average core size found by TEM is 7.2 ± 0.5 nm. The number-average hydrodynamic size from the elution time of 6.6 min is 6.7 nm with a range of sizes (half-width at half-height, HWHH) from 5.9 to 7.6 nm. The green curve (◇) corresponds to a neat toluene mobile phase. The red curve (○) shows that no elution occurs with only oleic acid in the mobile phase, while the blue curve (□) has hexadecylamine in the toluene phase.

As shown in Figures 8 and 9, only hexadecylamine produced a relatively sharp elution peak for samples Fe070301 and Fe112601. Although the stabilizer formed by the imide linkage between OA and OY allows adequate particle dispersion in dilute solution, the polystyrene column separates the Fe clusters from the stabilizer effectively preventing their complete elution from this column. The presence of a small amount of hexadecylamine in the mobile toluene phase helps to eliminate this effect. This effect is similar to that observed in transition metal clusters such as Ag, Au, or Pt in which alkanethiols improve cluster elution and peak shape.[24] Addition of oleic acid, hexadecylamine, or both to the cluster solution itself was

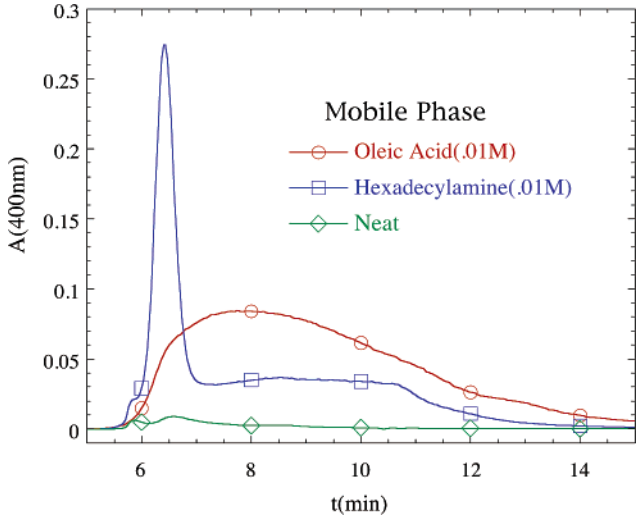

Figure 9. Absorbance chromatogram of Fe112601 nanoparticle sample of which the average core size by TEM is 5.8 ± 0.5 nm. The hydrodynamic size from the peak elution time of 6.4 min is 7.6 nm with a range (HWHH) from 6.7 to 8.6 nm. The green curve (◇) corresponds to a pure toluene mobile phase, which allows very little cluster elution. The red curve (○) shows that strong chemical interaction between clusters and column occurs with only oleic acid in the mobile phase, while the blue curve (□) has hexadecylamine in the neat toluene phase and produces a sharper elution peak with reduced tailing.

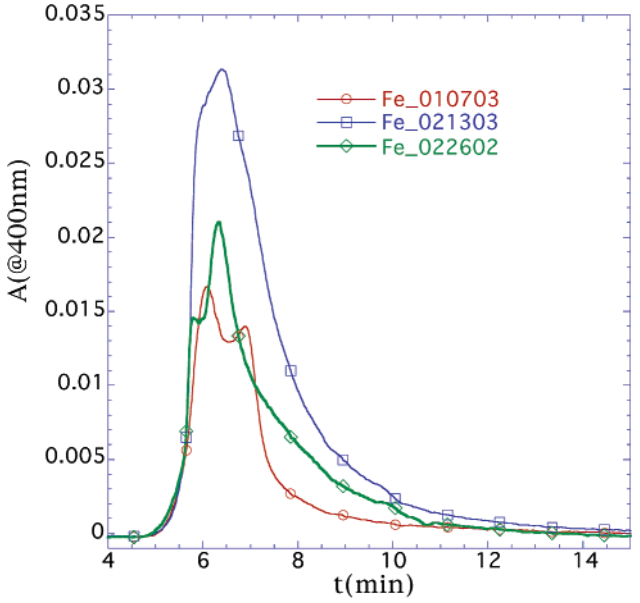

Figure 10. Absorbance vs elution time for three Fe samples, Fe010703 (red curve, ○), Fe021303 (blue curve, □), and Fe022602 (green curve, ◇). The mobile phase was oleic acid (0.015M)/oleic amine (0.016 M) in toluene. Sample Fe010703 has peaks corresponding to $D_h = 5.6$ and 9.2 nm, sample F021303 has $D_h = 7.6$ nm, and sample Fe022602 has $D_h = 8.1$ nm.

ineffective at stabilizing the Fe clusters because little or no elution occurred, demonstrating that the observed improvement in elution was due to a dynamic equilibrium between free and bound surfactant.

The hypothesis of the formation of a link between the two surfactants added for Fe nanoparticles was confirmed by the observation of an elution peak (not shown) at time matching that of an OA/OY= 0.015:0.016 M sample reacted in toluene and then injected into a pure toluene mobile phase. The detection of this stabilizer complex was accomplished using an on-line refractive index detector, which does not require that chemical analyte absorb visible or UV light. The elution time observed for the OA/OY did not match that of either pure OA or pure OY. The concentration of the OA/OY as determined by the refractive index peak area was very similar for samples of identical Fe concentrations (as determined by X-ray fluorescence) and was about 6×10^{-3} M.

SEC can separate by both size and shape, so the size quoted above might not be expected to agree with simple TEM cross-sectional measurements. In Figure 8, the difference between the number-average size as determined by TEM and SEC is small. In Figure 9, sample Fe112601 has more tailing in its chromatogram indicating that some particle/column interactions may be occurring. This effect is largest when only oleic acid is present in the mobile phase. More importantly, this demonstrates that OA by itself is a poor stabilizer for Fe clusters, though it is quite effective for metal oxide clusters. The average TEM size for sample Fe112601 is smaller than the hydrodynamic SEC size by 1.4 nm. As in Fe070301 shown in Figure 8, the effect of various surfactants added to the mobile phase is dramatic, indicating the possibility of residual chemical affinity between the Fe clusters and the polystyrene column.

In the case of larger Fe clusters, SEC is most useful for examining the range of sizes in a sample as shown in three samples the average size of which by TEM is similar. In Figure 10, sample Fe010703 with an average TEM size of 8.5 nm has a range of sizes (full width at half-height) from 5.2 to 12.5 nm with a peak value of 9.5 nm. TEM of this sample shows an average cross-sectional diameter of 8.6 nm and a standard deviation in the ordered regions of the grid of ±1 nm. Particles were observed outside these ordered regions with sizes as small as 3.6 nm and as large as 12.7 nm consistent with the spread in sizes observed in the elution curve of Figure 10. In the case of sample Fe022602, a clear bimodal distribution was observed by TEM with average sizes of 11−13 nm and 5−6 nm, consistent with the TEM image of Figure 3b. This sample shows an average size at the elution peak of $D_h = 8.1$ nm and a range of sizes from 4.9 to 12.5 nm. It is likely that the long tails observed in these elution curves are due to specific chemical interactions between the clusters and the column, so the simple log $D_h \approx t$ relation may not be valid for this time regime for these weakly passivated clusters. This means that the average size obtained by assuming a pure SEC elution mechanism will be too small. However, we found very little shift in the elution time at the peak apex when different stabilizers were used in the mobile phase, so it appears that the peak positions may reflect the number-average hydrodynamic diameter in solution. Total cluster exclusion from the pores occurs near $t = 5.0$ min, so the clusters are penetrating into the pores, but we are near the size limit of $D_h = 10$ nm for this column, so this may also explain the larger size observed in TEM for two of the samples.

D. X-ray Fluorescence and Particle Concentration. From the total amount of Fe and the particle sizes found by TEM or SEC, the particle concentration in solution can be estimated provided the sample is monodisperse. These concentration measurements allow us to determine the magnetic response of our samples in emu/g with high accuracy. The most reliable results for the particle concentrations were obtained from X-ray fluorescence studies.

Table 1 shows the results for several different samples. The data refer to the particles in their as-made concentrations, though for the actual measurements the particles have been redispersed in toluene. The particle concentrations are estimated using the average TEM diameter, and the results would be skewed to slightly lower values if the measured distributions of the particle diameters were used instead.

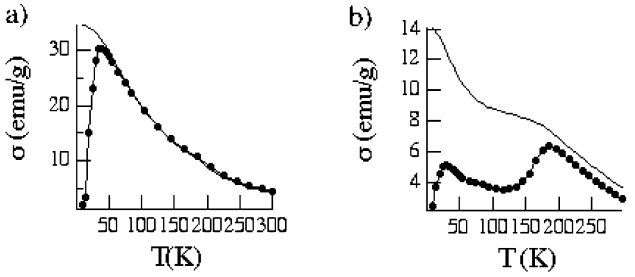

Figure 11. Zero-field- (lower) and field-cooled (upper) curves of the specific magnetization versus temperature for (a) heterogeneously nucleated 7.0 ± 0.8 nm Fe particles (sample Fe101801) and (b) homogeneously nucleated 11.2 ± 1.0 nm particles (sample Fe022602). The samples were roughly 0.01 vol % dispersions. The field-cooled data were taken with $H = 200$ Oe.

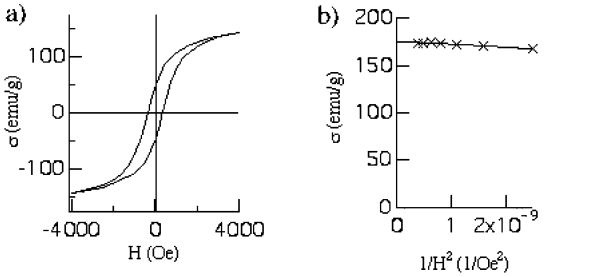

Figure 12. Hysteresis loop (a) for a 0.01 vol % dispersion of 7.0 ± 0.8 nm Fe particles (sample Fe 101801) measured at 10 K. Data were taken up to ±50 kOe, but only the low-field portion of the curve is shown. Panel b shows a plot of extrapolation used to determine σ_s.

The results of X-ray fluorescence studies on heterogeneously nucleated samples were compared to the Pt and Fe concentrations expected from the abundance of the starting materials in the syntheses. For standard heterogeneously nucleated particles of ~7 nm diameter, such as sample Fe070301, the measured Fe concentration was on the order of 0.1 M. For comparison, from the volume of $Fe(CO)_5$ used in the synthesis of a typical sample and assuming quantitative yield, the Fe concentration was predicted to be 0.27 M. From the mass of a dried sample, washed multiple times with ethanol, the concentration was predicted to be 0.33 M. The high measured masses of the Fe samples indicate that some surfactant or diol remains on the particle surface despite repeated washing. The results of these particle concentration studies indicate that one-half to two-thirds of the surfactant mass remains on the particles after thorough washing.

The concentration of Pt was also determined for one of the heterogeneously nucleated samples, Fe112601. A quantitative yield would have given a concentration of 3.3×10^{-4} M in the particle solution, but the measured concentration was only 5×10^{-5} M. With such low relative abundance, the platinum is unlikely to have a significant affect on the magnetic properties of the heterogeneously nucleated particles studied here.

A yield of more than 80% was reported for iron oxide particles made by a process very similar to the homogeneous nucleation method described here.[21] The main difference with our particles is that we do not intentionally oxidize them at the end. Assuming a similar yield, the as-made particle concentration of sample Fe022602 is on the order of 10^{14} particles/mL, an order of magnitude lower than that for the heterogeneously nucleated samples. This sample had a bimodal size distribution, so the result could not be interpreted in a number of particles per cubic centimeter. This is consistent with their greater fraction of oxide, as seen in Figure 4, and their lack of ferrofluids response. Because the first stage of the syntheses has approximately the same amount of $Fe(CO)_5$, the difference in particle concentrations is associated with the higher concentration of cluster nuclei with the Pt seeding. The smaller variations among different heterogeneously nucleated samples could arise from variations in the small amount of the Pt reagent introduced into the reaction flask.

E. Magnetic Measurements and the Oxide Fraction. *E.1. Blocking Temperatures.* Figure 11 shows the field-cooled and zero-field-cooled magnetization curves for dilute samples of heterogeneously and homogeneously nucleated particles. In a zero-field-cooled curve, the initial rise in moment with temperature occurs as the increased thermal energy enables particles to overcome the energy barrier to alignment with the applied field. Above the blocking temperature, the thermal energy is sufficient to randomize the moments within the measurement time, and the measured moment decreases. The field-cooled curve will either be flat or show decreasing moment as the temperature increases to T_B, as the particles are not frustrated, being frozen into alignment with the field during cooling.

For the 7 nm heterogeneously nucleated particles, T_B is approximately 35 K. In contrast, the homogeneously nucleated particles show two peaks in the zero-field-cooled curve at 30 and 185 K. These peaks represent the blocking temperatures of the Fe and the ferrimagnetic iron oxide phases. The failure of the two curves to meet at high T indicates that the dispersion does not fully equilibrate within the measurement time in these samples.

E.2. Saturation Magnetization and the Oxide Fraction. The saturation magnetization of dilute samples of the nanoparticles was used to estimate the proportion of Fe and iron oxide in particles of different sizes made by either the heterogeneous or homogeneous nucleation method. Iron and iron oxides are magnetically distinguishable by the difference in their specific saturation magnetizations, $\sigma_s = 220$ emu/g for bulk Fe and $\sigma_s = 84$ emu/g for bulk Fe_3O_4.[10] The value of the particle specific magnetization σ_s (equal to the saturation magnetization M_s in emu/cc times the density) as a mass-weighted average of the relative contributions is given by[8]

$$\sigma_{s,pt} m_{pt} = \sigma_{s,Fe} m_{core} + \sigma_{s,ox} m_{shell} \quad (1)$$

Here m_{pt} is the total mass of the particle, m_{core} is the mass of the Fe core, and m_{shell} is the mass of the oxide shell; $\sigma_{s,pt}$, $\sigma_{s,Fe}$, and $\sigma_{s,ox}$ are the specific saturation magnetizations of the particles, bulk Fe, and bulk Fe_3O_4. Assuming the bulk densities are valid for the nanoparticles and using the measured σ_s for a particle sample and the average particle radius found from TEM, one can make an estimate of the thickness of the oxide layer. If γ-Fe_2O_3 were present instead of Fe_3O_4, as has been suggested by many Mössbauer experiments on iron oxide nanoparticles, σ_{shell} would be lower and the thickness of the oxide shell would be reduced. If the nanocrystalline oxide had a lower density than in the bulk phase, this would also reduce our estimates of the oxide shell thickness.

To experimentally determine the specific saturation magnetization σ_s for the nanoparticles, the measured $\sigma(H)$ from the hysteresis loop was plotted versus $1/H^2$. The σ_s is found by extrapolating to the infinite field limit ($1/H^2 = 0$)[25], as shown in Figure 12. In the case of sample Fe101801, the measured magnetization at a field of 50 kOe was 173 emu/g, but the extrapolated value for σ_s was 175 emu/g. Substituting this value into eq 1 yields a 5.8 nm diameter core. The corresponding oxide shell thickness of 0.6 nm is an upper limit because the oxide contribution to σ_s is probably overestimated. Spin canting

TABLE 2: Particle Magnetizations and Effective Oxide Shell Thicknesses

sample	TEM diameter (nm)	σ_s (emu/g)	Fe core diameter (nm)	oxide shell thickness (nm)
Fe101801	7.0 ± 0.7	175	5.8	0.6
Fe090501	9.2 ± 0.7	200	8.4	0.4
Fe022602	11.2 ± 1.0	132	7.0	2.1

effects almost certainly prevent the Fe_3O_4 shell from reaching the bulk value.

Table 2 shows the results of measurements on other samples. Here the analysis has been done assuming that the particles have an iron core and Fe_3O_4 shell, though a core−shell morphology was not observed by TEM. The heterogeneously nucleated particles have relatively thin oxide shells, on the order of half a nanometer. This is still thicker than expected for the "ideal" case, in which only the surface atoms bonded to surfactant molecules would not be Fe^0, but much less than for the homogeneously nucleated particles. It is not entirely obvious that the homogeneously nucleated particles will have a core−shell morphology because they appear to be formed with a considerable amount of oxide. While two distinct phases are observed in diffraction and magnetic measurements, it is still unclear how they are distributed through the particles.

IV. Conclusions

Iron-based nanoparticles were prepared by high-temperature solution-phase syntheses using heterogeneous and homogeneous nucleation, producing particles with markedly different properties. Electron diffraction showed greater crystallinity and a higher degree of oxidation for the homogeneously nucleated particles. Flocculation and annealing experiments showed that the heterogeneously nucleated particles were not significantly oxidized as-made. The homogeneously nucleated particles have a distinct intermediate stage, attributed to iron oleate formation, which may be responsible. Size-exclusion chromatography on particles with different surfactant coatings showed that with mixtures of oleic and oleylamine, a peptide-like link is formed between them. SEC also revealed that this double-chained surfactant, as well as oleic acid alone, will adsorb and desorb regularly from the particle surface. Only hexadecylamine-passivated particles showed a narrow distribution of retention times. X-ray fluorescence showed that the Fe concentration was an order of magnitude lower in the homogeneously nucleated particle solutions, as-made. This result is attributed to the smaller number of cluster nuclei. Magnetically, the properties of the heterogeneously nucleated particles are dominated by those of their iron cores, while the homogeneously nucleated particles show a combination of features expected for both iron and iron oxide phases. Because of this, even with a reduced degree of crystallinity, the heterogeneously nucleated particles have higher magnetic moments.

The specific magnetization of the particles made by different methods was found by combining the particle size results obtained by TEM, the particle concentrations determined from calibrated X-ray fluorescence, and the hysteresis loops of particle samples. The results show high values of the specific magnetization for heterogeneously nucleated particles. When analyzed in terms of an effective core−shell model, these particles have an oxide shell thickness on the order of 0.5 nm. The presence of some degree of surface oxidation is expected for any Fe nanoparticles outside of ultrahigh vacuum conditions. It is unsurprising that the highest magnetizations previously reported for Fe-based nanoparticles were measured for large particle sizes, $D_{avg} = 20$ nm for the particles of ref 8 and 30 nm for those of ref 15. Here we have demonstrated that high magnetizations are also feasible in much smaller particles. We have identified the limits to improvement of the magnetization and described techniques for standardizing quantitative measurements on magnetic nanoparticles.

Acknowledgment. S.A.M. thanks the National Science Foundation (Grants CTS9800127 and CTS-0227645) and the Petroleum Research Fund of the American Chemical Society (Grant ACS-PRF-37578-AC5) for financial support. The work at Sandia National Laboratories was supported by the Division of Materials Science and Engineering, Office of Science, U.S. Department of Energy under Contract DE-AC04-AL8500. Sandia is a multiprogram laboratory operated by Sandia Corporation, a Lockheed-Martin Company, for the U.S. Department of Energy.

References and Notes

(1) Jorgensen, F. *The Complete Handbook of Magnetic Recording*; McGraw-Hill: New York, 1995.
(2) Rosensweig, R. E. *AIAA J.* **1966**, *4*, 1751.
(3) Molday, R. S.; Mackenzie, D. *J. Immunol. Methods* **1982**, *52*, 353−367.
(4) Tiefenauer, L. X.; Tscgirky, A.; Kuhne, G.; Andres, R. Y. *Magn. Reson. Imaging* **1996**, *14*, 391−402.
(5) Elliott, D. W.; Zhang, W.-X. *Environ. Sci. Technol.* **2001**, *35*, 4922−4926.
(6) Billas, I. M. L.; Chatelain, A.; de Heer, W. A. *Science* **1994**, *265*, 1682.
(7) Sun, S.; Murray, C. B.; Weller, D.; Folks, L.; Moser, A. *Science* **2000**, *287*, 1989.
(8) Gangopadhyay, S.; Hadjipanayis, G. C.; Sorensen, C. M.; Klabunde, K. J.; Papaefthymiou, V.; Kostikas, A. *Phys. Rev. B* **1992**, *45*, 9778.
(9) Massart, R. *IEEE Trans. Mag.* **1981**, *17*, 1247.
(10) O'Handley, R. C. *Modern Magnetic Materials, Principles and Applications*; John Wiley &Sons: New York, 2000; p 125.
(11) Fievet, F. *Surfactant Sci. Ser.* **2000**, 92.
(12) Giri, A. K.; Chowdary, K. M.; Majetich, S. A. *Mater. Phys. Mech.* **2000**, *1*, 1−10.
(13) Griffiths, C. H.; O'Horo, M. P.; Smith, T. W. *J. Appl. Phys.* **1979**, *50*, 7108.
(14) Hess, P. H.; Parker, P. H., Jr. *J. Appl. Polym. Sci.* **1966**, *10*, 1915−1927.
(15) Grinstaff, M. W.; Salamon, M. B.; Suslick, K. S. *Phys. Rev. B* **1993**, *48*, 269.
(16) Jönsson, P. E.; Felton, S.; Svedlindh, P.; Norblad, P.; Hansen, M. F. *Phys. Rev. B* **2001**, *64*, 212402.
(17) van Wonterghem, J.; Mørup, S.; Charles, S. W.; Wells, S.; Villadsen, J. *Phys. Rev. Lett.* **1985**, *55*, 410−413.
(18) Nakatani, I.; Hijikata, M.; Ozawa, K. *J. Magn. Magn. Mater.* **1993**, *122*, 10.
(19) Burke, N. A. D.; Stöver, H. D. H.; Dawson, F. P. *Chem. Mater.* **2002**, *14*, 4752−4761.
(20) Bentzon, M. D.; Thølen, A. R. *Ultramicroscopy* **1991**, *38*, 105.
(21) Hyeon, T.; Lee, S. S.; Park, J.; Chung, Y.; Bin Na, H. *J. Am. Chem. Soc.* **2001**, *123*, 12798.
(22) Sahoo, Y.; Pizem, H.; Fried, T.; Golodnitsky, D.; Bustein, L.; Sukenik, C. N.; Markovich, G. *Langmuir* **2001**, *17*, 7907−7911.
(23) Wilcoxon, J. P.; Martin, J. E.; Provencio, P. *J. Chem. Phys.* **2001**, *115*, 998.
(24) Wilcoxon, J. P.; Craft, S. A. *Nanostruct. Mater.* **1997**, *9*, 85−88.
(25) Skomski, R.; Coey, J. M. D. *Permanent Magnetism*; Institute of Physics Publishing: Bristol, U.K., Philadelphia, PA, 1999; p 162.